KURENAI

Kyoto University Research Information Repository

KYOTO UNIVERSITY

Title	Spin 3/2 pentaquarks in anisotropic lattice QCD
Author(s)	Ishii, N.; Doi, T.; Nemoto, Y.; Oka, M.; Suganuma, H.
Citation	Physical Review D (2005), 72(7)
Issue Date	2005-10-10
URL	http://hdl.handle.net/2433/198863
Right	© 2005 American Physical Society
Type	Journal Article
Textversion	publisher

Kyoto University

Spin 3/2 pentaquarks in anisotropic lattice QCD

N. Ishii,[1,*] T. Doi,[2,†] Y. Nemoto,[3,‡] M. Oka,[1,§] and H. Suganuma[4,∥]

[1]*Department of Physics, H-27, Tokyo Institute of Technology, 2-12-1 Oh-okayama, Meguro, Tokyo 152-8551, Japan*
[2]*RIKEN BNL Research Center, Brookhaven National Laboratory, Upton, New York 11973, USA*
[3]*Department of Physics, Nagoya University, Furo, Chikusa, Nagoya 464-8602, Japan*
[4]*Department of Physics, Kyoto University, Kitashirakawaoiwake, Kyoto 606-8502, Japan*

High-precision mass measurements of a pentaquark (5Q) Θ^+ in the $J^P = 3/2^\pm$ channels are performed in anisotropic quenched lattice QCD. A large number of gauge configurations ($N_{\mathrm{conf}} = 1000$) are prepared for the standard Wilson gauge action at $\beta = 5.75$ and the $O(a)$ improved Wilson (clover) quark action is employed for $\kappa = 0.1210(0.0010)0.1240$ on a $12^3 \times 96$ lattice with the renormalized anisotropy as $a_s/a_t = 4$. The Rarita-Schwinger formalism is adopted for interpolating fields. We examine several interpolating fields with isospin $I = 0$, such as (a) the NK^*-type, (b) the color-twisted NK^*-type, and (c) the diquark-type operators. After chiral extrapolation, we obtain massive states, $m_{5\mathrm{Q}} \simeq 2.1$–$2.2$ GeV in $J^P = 3/2^-$, and $m_{5\mathrm{Q}} = 2.4$–2.6 GeV in $J^P = 3/2^+$. Analyses using the hybrid boundary condition method are performed to determine whether these states are compact 5Q resonances or two-hadron scattering states. No compact 5Q resonance state is found below 2.1 GeV.

I. INTRODUCTION

The recent discovery of a manifestly exotic baryon $\Theta^+(1540)$ by the LEPS group at SPring-8 has made a great impact on the exotic hadron physics [1]. Apart from the other pentaquark baryon candidates, $\Xi^{--}(1862)$ [2] and $\Theta_c(3099)$ [3], several exotic hadrons have also been discovered, such as $X(3872)$, $D_s(2317)$, $S_0(3115)$, $X(3940)$, and $Y(3840)$ [4].

$\Theta^+(1540)$ is supposed to have a baryon number $B = 1$, a charge $Q = +1$, and a strangeness $S = +1$. Since $uudd\bar{s}$ is the minimal quark content to implement these quantum numbers, $\Theta^+(1540)$ is a manifestly exotic pentaquark (5Q) state. Such a pentaquark had been examined theoretically several times before the experimental discovery [5–9]. In particular, Ref. [5] provides a direct motivation for the experimental search [1]. The discovered peak in the nK^+ invariant mass is centered at 1.54 ± 0.01 GeV with a width smaller than 25 MeV. At the present stage, some groups have confirmed the LEPS discovery[10–13], while others have reported null results [14]. It will hence take a while to establish the existence or nonexistence of $\Theta^+(1540)$ experimentally [15]. Reference [12] indeed claims that Θ^+ must have $I = 0$, since no Θ^{++} is observed in the pK^+ invariant mass spectrum.

Enormous theoretical efforts have been devoted to the study of 5Q baryons [5–9,16–54]. One of the most challenging problems in understanding its structure is its extremely narrow decay width, which is reported to be $\Gamma \lesssim 1$ MeV [55]. Various physical ideas have been pro-

posed: (1) the $I = 2$ possibility [51], (2) the Jaffe-Wilczek's diquark picture [22], (3) the $\pi K N$ heptaquark picture [29,56], (4) the string picture [40,41], and (5) the $J^P = 3/2^-$ possibility [21,28]. Although each of them provides a mechanism to explain the narrow decay width, none of them can describe all the known properties of $\Theta^+(1540)$ simultaneously.

In this paper, we concentrate on the $J = 3/2$ possibility, in particular, we consider $J^P = 3/2^-$. Note that the spin of $\Theta^+(1540)$ has not yet been determined experimentally. In the constituent quark picture, the narrow decay width of $J^P = 3/2^-$ pentaquark is easily understood [21,28]. In that case, we expect the natural ground-state configuration to be $(0s)^5$, where all five quarks are in their orbit of lowest energy. While two spin states, $J^P = 1/2^-$ and $3/2^-$, are available, the $J^P = 3/2^-$ state can decay only to the d-wave NK scattering state, which has no overlap with the $(0s)^5$ configuration. Thus the decay is allowed only through its subdominant d-wave configuration, and the decay width is suppressed. Note that it is further suppressed by the d-wave centrifugal barrier, leading to a significantly narrow decay width of $J^P = 3/2^-$ pentaquarks. A possible disadvantage of the $J^P = 3/2^-$ assignment is that such a state tends to be massive due to the color-magnetic interaction in the constituent quark models, which seems to be the reason why so few effective model studies for spin 3/2 pentaquarks have been available [28,43–51,53,54]. However, it is not clear whether these conventional frameworks are applicable to a new exotic 5Q system as $\Theta^+(1540)$ without involving any modifications. Indeed, a model was proposed where a part of the role of the color-magnetic interaction can be played by the flavor-spin interaction, which makes the mass splitting between the $1/2^-$ and the $3/2^-$ states smaller [45].

There have been several lattice QCD calculations of 5Q states by now [57–67]. However, all these studies are

*Email address: ishii@rarfaxp.riken.jp
†Email address: doi@quark.phy.bnl.gov
‡Email address: nemoto@hken.phys.nagoya-u.ac.jp
§Email address: oka@th.phys.titech.ac.jp
∥Email address: suganuma@th.phys.titech.ac.jp

restricted to the $J^P = 1/2^\pm$ channels except for the one in Ref. [67]. Enormous efforts are being devoted to more accurate studies of $J^P = 1/2^\pm$ states, using the variational technique to extract multiple excited states, among which a compact resonance state is sought for. Indeed, quite large scale calculations are planned [68] attempting to elucidate some of the mysterious natures of $\Theta^+(1540)$ such as its diquark structure and/or nonlocalities in interpolating fields. Here, we emphasize again that these studies are aiming at $J^P = 1/2^\pm$ states, not at $3/2^\pm$ states.

In this paper, we present anisotropic lattice QCD results on 5Q states in the $J^P = 3/2^\pm$ channels using a large number of gauge configurations as $N_{\rm conf} = 1000$. We adopt the standard Wilson gauge action at $\beta = 5.75$ on the $12^3 \times 96$ lattice with the renormalized anisotropy $a_s/a_t = 4$. The anisotropic lattice is known to be a powerful tool for high-precision measurements of temporal correlators [69–72]. The large number of gauge configurations $N_{\rm conf} = 1000$ plays a key role in our calculation, because 5Q correlators in the $J^P = 3/2^\pm$ channels are found to be quite noisy. For quark action, we adopt the $O(a)$-improved Wilson (clover) action with four values of the hopping parameter, $\kappa = 0.1210(0.0010)0.1240$. One of the aims of our calculation is to examine how the results depend on the choice of interpolating field operators. We employ three types of interpolating fields: (a) the NK^* type, (b) the (color-)twisted NK^* type, and (c) a diquark type, and adopt a smeared source to enhance the low-lying spectra.

In the $J^P = 3/2^-$ channel, we obtain a massive state at $m_{5Q} \simeq 2.1$–2.2 GeV except for the case of the diquark-type interpolating field. The latter involves considerable statistical error. In the $J^P = 3/2^+$ channel, we obtain a state at $m_{5Q} \simeq 2.4$–2.6 GeV. None of these 5Q states appear below the NK threshold on the current lattice, which is raised by about 200–250 MeV due to the finite extent of the spatial lattice as $L \simeq 2.15$ fm. To clarify whether or not the observed 5Q states are compact resonance, we perform analyses with the hybrid boundary condition (HBC) method, which was recently proposed in Ref. [61]. HBC analyses indicate that there is no compact 5Q resonance in either of the $J^P = 3/2^\pm$ channels.

The paper is organized as follows. In Sec. II, we discuss the general formalism. We begin by introducing several types of interpolating fields, determining their parity transformation properties. We next consider the temporal correlator and its spectral decomposition. We finally discuss the two-particle scattering states which appear in 5Q spectra, and introduce the HBC to examine whether or not a state we are interested in is a compact resonance state. Section III is devoted to the description of the lattice action and parameters. In Sec. IV, we present the numerical results for the $J^P = 3/2^\pm$ channels in the standard periodic boundary condition (PBC). We present the 5Q correlators of various interpolating fields, i.e., the NK^* type, the

(color-)twisted NK^* type, and the diquark type. In Sec. V, we attempt to determine whether these 5Q states are compact 5Q resonance states or two-particle scattering states by using the HBC. In Sec. VI, a summary and conclusions are given.

II. GENERAL FORMALISMS

A. Interpolating fields

We consider an isoscalar interpolating field of NK^* *type* in the Rarita-Schwinger form [73–75] given by

$$\psi_\mu \equiv \epsilon_{abc}(u_a^T C \gamma_5 d_b)u_c \cdot (\bar{s}_d \gamma_\mu d_d) - \epsilon_{abc}(u_a^T C \gamma_5 d_b)d_c \cdot (\bar{s}_d \gamma_\mu u_d), \quad (1)$$

where μ denotes the Lorentz index, $a - d$ refers to the color indices, and $C = \gamma_4 \gamma_2$ denotes the charge conjugation matrix. Unless otherwise indicated, the gamma matrices are represented in the Euclidean form given in Ref. [76].

We study also the *(color-)twisted NK^* type* interpolating field given by

$$\psi_\mu \equiv \epsilon_{abc}(u_a^T C \gamma_5 d_b)u_d \cdot (\bar{s}_d \gamma_\mu d_c) - \epsilon_{abc}(u_a^T C \gamma_5 d_b)d_d \cdot (\bar{s}_d \gamma_\mu u_c), \quad (2)$$

which is analogous to the one originally proposed in Ref. [57] to study $J^P = 1/2^P$ 5Q states. It has a slightly more elaborate color structure than Eq. (1), suggesting somewhat stronger coupling to a genuine 5Q state, if it exists.

We also consider diquark-type interpolating fields proposed in Ref. [36]. For instance, we may choose the following interpolating field [58]:

$$\psi_\mu \equiv \epsilon_{abc}\epsilon_{def}\epsilon_{cfg}(u_a^T C \gamma_5 d_b)(u_d^T C \gamma_5 \gamma_\mu d_e)C\gamma_5 \bar{s}_g. \quad (3)$$

The first factor corresponds to a scalar diquark (color $\bar{\mathbf{3}}$, $I = 0$, $J^P = 0^+$), which may play important roles in hadron physics [77]. The second factor corresponds to a vector diquark (color $\bar{\mathbf{3}}$, $I = 0$, $J^P = 1^-$). Note that the axial-vector diquark (color $\bar{\mathbf{3}}$, $I = 1$, $J^P = 1^+$) is not suitable because of its isovector nature. Unless otherwise indicated, we refer to Eq. (3) as the *diquark-type* interpolating field. We may also consider another interpolating field of diquark type:

$$\psi_\mu \equiv \epsilon_{abc}\epsilon_{def}\epsilon_{cfg}(u_a^T C d_b)(u_d^T C \gamma_5 \gamma_\mu d_e)C\bar{s}_g, \quad (4)$$

which consists of a pseudoscalar diquark (color $\bar{3}$, $I = 0$, $J^P = 0^-$) and a vector diquark. However, actual lattice QCD calculations show that the correlator of Eq. (4) is afflicted with huge statistical errors. A possible reason for this is that neither of the two diquark factors of Eq. (4), the pseudoscalar diquark and the vector diquark, survive in the nonrelativistic limit while, in Eq. (3), the scalar diquark is allowed in the nonrelativistic limit. Hence, we do not consider Eq. (4) in this paper.

Under the spatial reflection, the quark field is transformed as

$$q(\tau, \vec{x}) \to \gamma_4 q(\tau, -\vec{x}), \qquad (5)$$

and the spatial components of the interpolating fields Eqs. (1)–(3) as

$$\psi_i(\tau, \vec{x}) \to -\gamma_4 \psi_i(\tau, -\vec{x}), \qquad (6)$$

for $i = 1, 2, 3$.

B. 5Q correlators and parity projection

We consider the Euclidean temporal correlator

$$G_{\mu\nu}(\tau) \equiv \sum_{\vec{x}} \langle \psi_\mu(\tau, \vec{x}) \bar{\psi}_\nu(0, \vec{0}) \rangle, \qquad (7)$$

where $\sum_{\vec{x}}$ projects the total 5Q momentum to zero. Since the spin $3/2$ contribution from the temporal component of the Rarita-Schwinger spinor vanishes in the rest frame, we can restrict ourselves to the spatial parts, i.e., $\mu\nu = 1, 2$, and 3. Now, Eq. (7) is decomposed in the following way:

$$G_{ij}(\tau) = \mathbf{P}_{ij}^{(3/2)} G^{(3/2)}(\tau) + \mathbf{P}_{ij}^{(1/2)} G^{(1/2)}(\tau), \qquad (8)$$

where i, j ($= 1, 2$, and 3) denote the spatial part of the Lorentz indices, $\mathbf{P}^{(3/2)}$ and $\mathbf{P}^{(1/2)}$ denote the projection matrices onto the spin $3/2$ and $1/2$ subspaces defined by

$$\mathbf{P}_{ij}^{(3/2)} \equiv \delta_{ij} - (1/3)\gamma_i\gamma_j, \qquad \mathbf{P}_{ij}^{(1/2)} \equiv (1/3)\gamma_i\gamma_j. \quad (9)$$

They satisfy the following relations as

$$\mathbf{P}_{ij}^{(3/2)}\mathbf{P}_{jk}^{(3/2)} = \mathbf{P}_{ik}^{(3/2)}, \qquad \mathbf{P}_{ij}^{(1/2)}\mathbf{P}_{jk}^{(1/2)} = \mathbf{P}_{ik}^{(1/2)},$$

$$\mathbf{P}_{ij}^{(1/2)} + \mathbf{P}_{ij}^{(3/2)} = \delta_{ij}, \qquad \mathbf{P}_{ij}^{(1/2)}\mathbf{P}_{jk}^{(3/2)} = \mathbf{P}_{ij}^{(3/2)}\mathbf{P}_{jk}^{(1/2)} = 0,$$

$$(10)$$

where summations over repeated indices are understood. $G^{(3/2)}(\tau)$ and $G^{(1/2)}(\tau)$ in Eq. (7) denote the spin $3/2$ and $1/2$ contributions to $G(\tau)$, respectively, which can be derived by applying the operators $\mathbf{P}^{(3/2)}$ and $\mathbf{P}^{(1/2)}$ on $G(\tau)$, respectively. [In our practical lattice QCD calculation, we construct the Rarita-Schwinger correlator $G_{ij}(\tau)$ for $i = 1, 2$, and 3 and $j = 3$ (fixed), and multiply $\mathbf{P}^{(3/2)}$ from the left to obtain $G^{(3/2)}(\tau)$.]

In the asymptotic region ($0 \ll \tau \ll N_t$), contaminations of excited states are suppressed. Considering the parity transformation property Eq. (6), $G^{(3/2)}(\tau)$ and $G^{(1/2)}(\tau)$ are expressed in this region as

$$G^{(3/2)}(\tau) = P_+\{|\lambda_{3/2^-}|^2 e^{-\tau m_{3/2^-}} + |\lambda_{3/2^+}|^2 e^{-(N_t-\tau)m_{3/2^+}}\}$$
$$- P_-\{|\lambda_{3/2^+}|^2 e^{-\tau m_{3/2^+}} + |\lambda_{3/2^-}|^2 e^{-(N_t-\tau)m_{3/2^-}}\},$$

$$G^{(1/2)}(\tau) = P_+\{|\lambda_{1/2^-}|^2 e^{-\tau m_{1/2^-}} + |\lambda_{1/2^+}|^2 e^{-(N_t-\tau)m_{1/2^+}}\}$$
$$- P_-\{|\lambda_{1/2^+}|^2 e^{-\tau m_{1/2^+}} + |\lambda_{1/2^-}|^2 e^{-(N_t-\tau)m_{1/2^-}}\},$$

$$(11)$$

where $P_\pm \equiv (1 \pm \gamma_4)/2$ denote the projection matrices onto the "upper" and "lower" Dirac subspaces, respectively. Here $m_{3/2^\pm}$ and $m_{1/2^\pm}$ denote the lowest-lying masses in the $J^P = 3/2^\pm$ and $1/2^\pm$ channels, respectively, while $\lambda_{3/2^\pm}$ and $\lambda_{1/2^\pm}$ represent couplings of the interpolating field to the lowest $J^P = 3/2^\pm$ and $1/2^\pm$ states, respectively. In Eq. (11), we adopt the antiperiodic boundary condition along the temporal direction. A brief derivation of Eqs. (8) and (11) is presented in the Appendix. The forward propagation is dominant in the region $0 < \tau \lesssim N_t/2$, while the backward propagation is dominant in the region $N_t/2 \lesssim \tau < N_t$. To separate the negative (positive) parity contribution, we restrict ourselves to the region $0 < \tau \lesssim N_t/2$, and examine the upper (lower) Dirac component.

C. Scattering states involved in 5Q spectrum

We consider baryon-meson scattering states which appear in the present 5Q spectrum. For $J^P = 3/2^\pm$ isoscalar pentaquarks, NK and NK^* scattering states play important roles. (ΔK states do not couple to the isoscalar channel.) These states are expressed as

$$|N(\vec{p}, s)K(-\vec{p})\rangle, \quad |N(\vec{p}, s)K^*(-\vec{p}, i)\rangle, \qquad (12)$$

where s and i denote the spin of the nucleon and K^*, and $\vec{p}$ denotes the spatial momentum allowed for a particular choice of the spatial boundary conditions. For instance, if these hadrons are subject to spatially periodic boundary conditions, their momenta are quantized as

$$p_i = 2n_i\pi/L, \qquad n_i \in \mathbb{Z}, \qquad (13)$$

where L denotes the spatial extent of the lattice. In contrast with this situation, if they are subject to spatially antiperiodic boundary conditions, their momenta are quantized as

$$p_i = (2n_i + 1)\pi/L, \qquad n_i \in \mathbb{Z}. \qquad (14)$$

We first perform the parity projections. The positive ("+") and the negative ("−") parity projections of Eq. (12) are obtained in the following way:

$$|NK(\pm)\rangle = |N(\vec{p}, s)K(-\vec{p})\rangle \mp |N(-\vec{p}, s)K(\vec{p})\rangle, \quad (15)$$

$$|NK^*(\pm)\rangle = |N(\vec{p}, s)K^*(-\vec{p}, i)\rangle \mp |N(-\vec{p}, s)K^*(\vec{p}, i)\rangle. \qquad (16)$$

Assuming that the interactions between N and K and between N and K^* are weak, their energies are approximated by

$$E_{NK} \simeq \sqrt{m_N^2 + \vec{p}^2} + \sqrt{m_K^2 + \vec{p}^2} \qquad (17)$$

and

$$E_{N^*K} \simeq \sqrt{m_N^2 + \vec{p}^2} + \sqrt{m_{K^*}^2 + \vec{p}^2}, \qquad (18)$$

respectively. The scattering states which couple to $J^P = 3/2^{\pm}$ pentaquarks are obtained by the spin $3/2$ projections of Eqs. (15) and (16). The d-wave NK states and the s-wave NK^* states can couple to the $J^P = 3/2^-$ pentaquark, while the p-wave NK states and NK^* states may couple to the $J^P = 3/2^+$ pentaquark.

The scattering states with vanishing spatial momentum $\vec{p} = \vec{0}$ are exceptional in the following sense. On the one hand, the positive parity states vanish, because the first terms coincide with the second terms in Eqs. (15) and (16) on the right-hand side. On the other hand, the negative parity states are constructed only from the spin degrees of freedom, i.e., the spin degrees of freedom of the nucleon in Eq. (15), and the spin degrees of freedoms of the nucleon and K^* in Eq. (16). By counting the degeneracy of the resulting states, it is straightforward to see that no d-wave states are contained, i.e., Eq. (15) only gives s-wave NK states in the $J^P = 1/2^-$ channel, and Eq. (16) only gives s-wave NK^* states in the $J^P = 1/2^-$ and $3/2^-$ channels.

D. Hybrid boundary condition

In order to determine whether the observed state is a compact 5Q resonance state or a scattering state of two particles, we use a novel technique recently proposed in Ref. [61]. We employ two distinct spatial boundary conditions (BC), i.e., the (standard) periodic BC and the hybrid BC, and compare the results. In the PBC, one imposes a spatially periodic BC on u, d, and s quarks. As a result, all the hadrons are subject to periodic BC. In this case, due to Eq. (13), all hadrons can take zero momentum, and the smallest nonvanishing momentum $\vec{p}_{\min}$ is of the form

$$(\pm 2\pi/L, 0, 0), \quad (0, \pm 2\pi/L, 0), \quad (0, 0, \pm 2\pi/L), \quad (19)$$

which gives

$$|\vec{p}_{\min}^{\text{PBC}}| = 2\pi/L. \qquad (20)$$

On the other hand, with HBC, we impose the spatially antiperiodic BC on u and d quarks, whereas the spatially periodic BC is imposed on the s quark. Since $N(uud, udd)$, $K(u\bar{s}, d\bar{s})$, and $K^*(u\bar{s}, d\bar{s})$ contain odd numbers of u and d quarks, they are subject to antiperiodic BC. Therefore, due to Eq. (14), N, K, and K^* cannot have a vanishing momentum with HBC. The smallest possible momentum $\vec{p}_{\min}$ is of the form,

$$(\pm\pi/L, \pm\pi/L, \pm\pi/L), \qquad (21)$$

hence,

$$|\vec{p}_{\min}^{\text{HBC}}| = \sqrt{3}\pi/L. \qquad (22)$$

In contrast, Θ^+ $(uudd\bar{s})$ is subject to spatially periodic BC, since it contains an even number of u and d quarks.

Therefore, a compact Θ^+ can have a vanishing momentum.

Switching from PBC, HBC affects the low-lying two-particle scattering spectrum. A drastic change is expected in the s-wave NK^* channel. With PBC, the energy of the lowest NK^* state is given as

$$E_{\min}^{\text{PBC}}(NK^*(s \text{ wave})) \simeq m_N + m_{K^*}, \qquad (23)$$

while, with HBC, since both N and K^* are required to have nonvanishing momenta $|\vec{p}_{\min}| = \sqrt{3}\pi/L$, the energy of the lowest NK^* state is raised to

$$E_{\min}^{\text{HBC}}(NK^*(s \text{ wave})) \simeq \sqrt{m_N^2 + 3\pi^2/L^2}$$
$$+ \sqrt{m_{K^*}^2 + 3\pi^2/L^2}. \qquad (24)$$

Note that the shift is typically of a few hundred MeV for $L \sim 2$ fm.

HBC affects NK (d wave), NK (p wave), and NK^* (p wave) as well. However, these changes are not as drastic as that in NK^* (s wave), because they are induced by the minor change in the minimum momentum from $|\vec{p}_{\min}| = 2\pi/L$ to $\sqrt{3}\pi/L$. With PBC, the energies of the lowest two-particle states are expressed as

$$E_{\min}^{\text{PBC}}(NK(p/d \text{ wave})) \simeq \sqrt{m_N^2 + 4\pi^2/L^2}$$
$$+ \sqrt{m_K^2 + 4\pi^2/L^2},$$
$$E_{\min}^{\text{PBC}}(NK^*(p \text{ wave})) \simeq \sqrt{m_N^2 + 4\pi^2/L^2}$$
$$+ \sqrt{m_{K^*}^2 + 4\pi^2/L^2}. \qquad (25)$$

In HBC, they are lowered to

$$E_{\min}^{\text{HBC}}(NK(p/d \text{ wave})) \simeq \sqrt{m_N^2 + 3\pi^2/L^2}$$
$$+ \sqrt{m_K^2 + 3\pi^2/L^2},$$
$$E_{\min}^{\text{HBC}}(NK^*(p \text{ wave})) \simeq \sqrt{m_N^2 + 3\pi^2/L^2}$$
$$+ \sqrt{m_{K^*}^2 + 3\pi^2/L^2}. \qquad (26)$$

Table I shows how the threshold energies are affected by the boundary conditions at each hopping parameter for a spatial lattice of size $L \simeq 2.15$ fm.

In contrast to the scattering states, HBC is not expected to affect a compact 5Q resonance Θ^+ as much. Since $\Theta^+(uudd\bar{s})$ can have vanishing momentum also with HBC, the shift of the pentaquark mass m_{5Q} originates only from the change in its intrinsic structure. In this case, the shift is expected to be less significant than the shift induced by the kinematic reason as it is the case in N, K, and K^*. We will now look for a compact 5Q resonance state by studying which states remain unaffected by HBC.

TABLE I. Numerical values of NK [Eq. (17)] and NK^* [Eq. (18)] thresholds for each hopping parameter κ in the physical unit GeV for the spatial lattice size $L \simeq 2.15$ fm under PBC and HBC. The rightmost column labeled as "Emp." shows the threshold energies for the physical values of the masses of N, K, and K^*: $m_N \simeq 0.94$ GeV, $m_K \simeq 0.5$ GeV, $m_{K^*} \simeq 0.89$ GeV. The scale unit is determined using the static quark potential with the Sommer scale $r_0^{-1} = 395$ MeV (see Sec. III for details).

κ		0.1210	0.1220	0.1230	0.1240	Emp.
NK^* (s wave)	PBC	2.996	2.815	2.633	2.445	1.830
NK^* (p wave)	PBC	3.222	3.052	2.883	2.710	2.163
NK (p/d wave)	PBC	2.987	2.806	2.624	2.438	1.865
NK^* (s/p wave)	HBC	3.167	2.995	2.823	2.647	2.084
NK (p/d wave)	HBC	2.924	2.739	2.553	2.363	1.770

III. LATTICE ACTIONS AND PARAMETERS

To generate gauge field configurations, we use the standard plaquette action on the anisotropic lattice of the size $12^3 \times 96$ as

$$S_G = \frac{\beta}{N_c} \frac{1}{\gamma_G} \sum_{x, i<j\leq3} \mathrm{Re\,Tr}\{1 - P_{ij}(x)\}$$
$$+ \frac{\beta}{N_c} \gamma_G \sum_{x, i\leq3} \mathrm{Re\,Tr}\{1 - P_{i4}(x)\}, \qquad (27)$$

where $P_{\mu\nu}(x) \in \mathrm{SU}(3)$ denotes the plaquette operator in the μ-ν plane. The lattice parameter and the bare anisotropy parameter are fixed as $\beta \equiv 2N_c/g^2 = 5.75$ and $\gamma_G = 3.2552$, respectively. These values are determined to reproduce the renormalized anisotropy as $\xi \equiv a_s/a_t = 4$ [69]. Adopting the pseudo-heat-bath algorithm, we pick up gauge field configurations every 500 sweeps after skipping 10 000 sweeps for the thermalization. We use a total of 1000 gauge field configurations to construct the temporal correlators. Note that the high statistics of $N_{\mathrm{conf}} = 1000$ is quite essential for our study, because the 5Q correlators for spin 3/2 states are found to be rather noisy. In fact, a preliminary analysis with less statistics $N_{\mathrm{conf}} \simeq 500$ leads to a spurious resonancelike state. (Such a tendency was reported at the Japan-U.S. Workshop on "Electromagnetic Meson Production and Chiral Dynamics," Osaka, Japan, 2005 [78].) The lattice spacing is determined from the static quark potential adopting the Sommer scale $r_0^{-1} = 395$ MeV $(r_0 \sim 0.5$ fm) as $a_s^{-1} = 1.100(6)$ GeV $(a_s \simeq 0.18$ fm). Note that the lattice size $12^3 \times 96$ corresponds to $(2.15\text{ fm})^3 \times (4.30\text{ fm})$ in the physical unit.

We adopt the $O(a)$-improved Wilson (clover) action on the anisotropic lattice for quark fields ψ and $\bar{\psi}$ as [70]

$$S_F \equiv \sum_{x,y} \bar{\psi}(x) K(x, y) \psi(y), \qquad (28)$$

$$K(x, y) \equiv \delta_{x,y} - \kappa_t\{(1 - \gamma_4)U_4(x)\delta_{x+\hat{4},y}$$
$$+ (1 + \gamma_4)U_4^\dagger(x - \hat{4})\delta_{x-\hat{4},y}\}$$
$$- \kappa_s \sum_i\{(r - \gamma_i)U_i(x)\delta_{x+\hat{i},y}$$
$$+ (r + \gamma_i)U_i^\dagger(x - \hat{i})\delta_{x-\hat{i},y}\}$$
$$- \kappa_s c_E \sum_i \sigma_{i4}F_{i4}\delta_{x,y} - r\kappa_s c_B \sum_{i<j}\sigma_{ij}F_{ij}\delta_{x,y},$$

where κ_s and κ_t denote the hopping parameters for the spatial and the temporal directions, respectively. The field strength $F_{\mu\nu}$ is defined through the standard clover-leaf-type construction. r denotes the Wilson parameter. c_E and c_B denote the clover coefficients. To achieve the tadpole improvement, the link variables are rescaled as $U_i(x) \to U_i(x)/u_s$ and $U_4(x) \to U_4(x)/u_t$, where u_s and u_t denote the mean-field values of the spatial and temporal link variables, respectively [70,71]. This is equivalent to the redefinition of the hopping parameters as the tadpole-improved ones (with tilde), i.e., $\kappa_s = \tilde{\kappa}_s/u_s$ and $\kappa_t = \tilde{\kappa}_t/u_t$. The anisotropy parameter is defined as $\gamma_F \equiv \tilde{\kappa}_t/\tilde{\kappa}_s$, which coincides with the renormalized anisotropy $\xi = a_s/a_t$ for sufficiently small quark mass at the tadpole-improved level [70]. For given κ_s, the four parameters r, c_E, c_B, and κ_s/κ_t should be, in principle, tuned so that the "Lorentz symmetry" is respected up to discretization errors of $O(a^2)$. Here, r, c_E, and c_B are fixed by adopting the tadpole-improved tree-level values as

$$r = \frac{1}{\xi}, \qquad c_E = \frac{1}{u_s u_t^2}, \qquad c_B = \frac{1}{u_s^3}. \qquad (29)$$

Only the value of $\kappa_t/\kappa_s(= \gamma_F \cdot (u_s/u_t))$ is tuned nonperturbatively by using the meson dispersion relation [70]. It is convenient to define κ as

$$\frac{1}{\kappa} \equiv \frac{1}{\tilde{\kappa}_s} - 2(\gamma_F + 3r - 4). \qquad (30)$$

Then the bare quark mass is expressed as $m_0 = \frac{1}{2}(1/\kappa - 8)$ in the spatial lattice unit in the continuum limit. This κ plays the role of the hopping parameter "κ" in the isotropic formulation; for details, see Refs. [70,71], where we take the lattice parameters. The values of the lattice parameters are summarized in Table II.

We choose four values of the hopping parameter as $\kappa = 0.1210$, 0.1220, 0.1230, and 0.1240, which correspond to $m_\pi/m_\rho = 0.81$, 0.78, 0.73, and 0.66, respectively. These values roughly cover the region $m_s \lesssim m \lesssim 2m_s$. For the temporal direction, we impose antiperiodic boundary conditions on all the quark fields. For spatial directions, we impose periodic boundary conditions on all the quarks, unless otherwise indicated. We refer to this boundary condition as "PBC."

By keeping $\kappa_s = 0.1240$ fixed for the s quark, and by changing $\kappa = 0.1210$–0.1240 for u and d quarks, we per-

TABLE II.   Parameters of the lattice simulation. The spatial lattice spacing a_s is determined by fixing the Sommer scale, $r_0^{-1} = 395$ MeV. The mean-field values of link variables (u_s and u_t) are defined in the Landau gauge. κ_c denotes the critical value of κ.

β	γ_G	a_s/a_t	a_s^{-1} (GeV)	Size	N_{conf}	u_s	u_t	γ_F	κ_c	Values of κ
5.75	3.2552	4	1.100(6)	$12^3 \times 96$	1000	0.7620(2)	0.9871(0)	3.909	0.12640(5)	0.1240, 0.1230, 0.1220, 0.1210

form the chiral extrapolation to the physical quark mass region. In the following part of the paper, we will use

$$(\kappa_s, \kappa) = (0.1240, 0.1220), \tag{31}$$

as a typical set of hopping parameters in presenting correlators and effective mass plots. For convenience, we show the obtained masses of π, ρ, K, K^*, N, and N^* ($J^P = 1/2^-$ baryon) for each hopping parameter κ together with their values at the physical quark mass in Table III. Here, the chiral extrapolations of masses of these particles are performed by a linear function in m_π^2. Unless otherwise indicated, we adopt the jackknife prescription to estimate the statistical errors.

We use a smeared source to enhance the low-lying spectra. To implement it, we employ a Gaussian smeared source after the Coulomb gauge fixing. The smearing technique after the Coulomb gauge fixing is an established method, which has been widely used in many papers [61,66,70,71,79–81]. As a smearing function, Refs. [79–81] have employed an exponential function, while Refs. [61,66,70,71] have employed a Gaussian function. We first perform the Coulomb gauge fixing of gauge configurations, and obtain quark propagators with a spatially extended source with the Gaussian size $\rho \simeq 0.4$ fm according to

$$q_{\text{smear}}(\tau, \vec{x}) \equiv \mathcal{N} \sum_{\vec{y}} \exp\left\{ -\frac{|\vec{x} - \vec{y}|^2}{2\rho^2} \right\} q(\tau, \vec{y}), \tag{32}$$

where $\mathcal{N}$ is an appropriate normalization factor. By using these smeared quark propagators, we construct the pentaquark correlators with smeared source and point sink. In the actual calculation, we modify Eq. (32) so that the smearing is consistent with the finite lattice size and the particular boundary condition.

TABLE III.   Masses of π, ρ, K, K^*, N, and N^* for each hopping parameter κ in the physical unit GeV. $\kappa_{\text{phys.}} \simeq 0.1261$ denotes the value of κ which achieves $m_\pi \simeq 0.14$ GeV.

κ	0.1210	0.1220	0.1230	0.1240	$\kappa_{\text{phys.}}$
m_π	1.007(2)	0.897(1)	0.785(2)	0.658(2)	0.140
m_ρ	1.240(4)	1.157(5)	1.074(7)	0.991(11)	0.823(13)
m_K	0.846(2)	0.785(1)	0.722(2)	0.658(2)	0.476(2)
m_{K^*}	1.119(6)	1.076(7)	1.033(9)	0.991(11)	0.902(15)
m_N	1.877(4)	1.739(3)	1.600(4)	1.454(5)	1.164(8)
m_{N^*}	2.325(18)	2.194(21)	2.059(28)	1.918(43)	1.648(53)

IV. NUMERICAL RESULTS ON 5Q SPECTRUM

In this section, we present our lattice QCD results on 5Q spectrum in the standard PBC.

A. $J^P = 3/2^-$ 5Q spectrum with PBC

We consider the spectrum of $J^P = 3/2^-$ pentaquarks. In Fig. 1, we show the effective mass plots for three interpolating fields, i.e., (a) the NK^* type, (b) the twisted NK^* type, and (c) a diquark type. The dotted lines indicate the s-wave NK^* and the d-wave NK thresholds, which happen to coincide in Fig. 1 for the spatial lattice size $L \simeq 2.15$ fm.

We define the effective mass as a function of τ by

$$m_{\text{eff}}(\tau) \equiv \log\left(\frac{G^{(3/2)}(\tau)}{G^{(3/2)}(\tau + 1)} \right), \tag{33}$$

where $G^{(3/2)}(\tau)$ denotes the temporal correlator. At sufficiently large τ, the correlator is dominated by the lowest-lying state with energy m as $G^{(3/2)}(\tau) \sim A e^{-m\tau}$. Then Eq. (33) gives a constant as $m_{\text{eff}}(\tau) \simeq m$. Thus a plateau in $m_{\text{eff}}(\tau)$ indicates that the correlator is saturated by a single state. In such cases, we can perform a single-exponential fit in the plateau region.

Figure 1(a) shows the effective mass plot for the NK^*-type interpolating field. In the region $0 \leq \tau \leq 24$, the contamination of the higher spectral contributions is gradually reduced, which is indicated by the decrease in $m_{\text{eff}}(\tau)$. There is a plateau in the interval $25 \lesssim \tau \lesssim 35$, where a single state is expected to dominate the 5Q correlator. Beyond $\tau \sim 36$, the statistical errors become large. In addition, the effect of the backward propagation becomes significant as we approach $\tau \sim 48$. Hence, we simply neglect the data for $\tau \gtrsim 36$, and perform a single-exponential fit in the region $25 \leq \tau \leq 35$. We obtain $m_{5Q} = 2.90(2)$ GeV, which is denoted by the solid line. One sees that the 5Q states appears above the s-wave NK^* and the d-wave NK thresholds.

Figure 1(b) shows the effective mass plot for the twisted NK^*-type interpolating field. There is a plateau in the interval $24 \lesssim \tau \lesssim 35$, where the single-exponential fit leads to $m_{5Q} = 2.89(1)$ GeV. The 5Q state is again above the s-wave NK^* and the d-wave NK thresholds.

Figure 1(c) shows the effective mass plot for the diquark-type interpolating field. We see that statistical errors are too large to identify a plateau unambiguously. Hence, we do not perform the fit. Note that this plot is obtained by using $N_{\text{conf}} = 1000$ gauge configurations. A
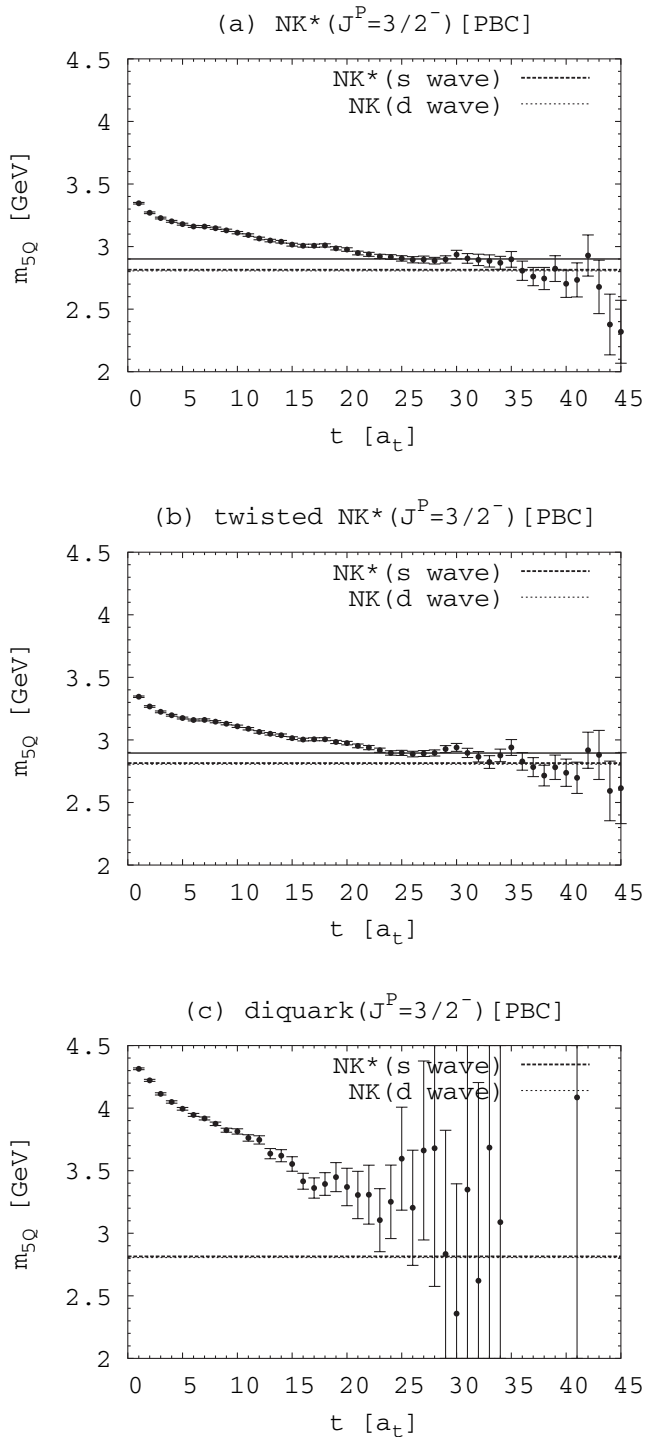
FIG. 1. The 5Q effective mass plots in the $J^P = 3/2^-$ channel in the standard PBC for three types of interpolating fields, i.e., (a) the NK^* type, (b) the twisted NK^* type, and (c) the diquark type. Equation (31) is adopted as a typical set of hopping parameters. The statistical error is estimated with the jackknife prescription. The dotted lines indicate the s-wave NK^* and the d-wave NK threshold in the spatial lattice size $L \simeq 2.15$ fm. Note that they accidentally coincide with each other. The solid lines denote the results of the single-exponential fit performed in each plateau region.
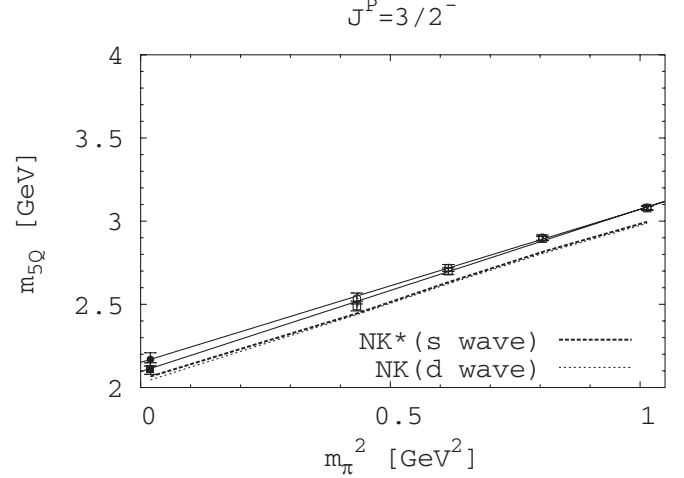
FIG. 2. m_{5Q} in the $J^P = 3/2^-$ channel against m_π^2 for the two interpolating fields, i.e., (circle) the NK^* type, (square) the twisted NK^* type. Open symbols denote the direct lattice QCD data, while the closed symbols and the solid lines represent the results of the chiral extrapolations to the physical quark mass region.

possible reason for such large noises is that the interpolating field Eq. (3) does not survive in the nonrelativistic limit due to its vector diquark component.

Now, we perform the chiral extrapolation. As mentioned before, we keep $\kappa = 0.1240$ fixed for the s quark, and vary $\kappa = 0.1210$–0.1240 for the u and d quarks. Figure 2 shows the 5Q masses in the $J^P = 3/2^-$ channel against m_π^2. Circles and squares denote the data obtained from the NK^*-type and the twisted NK^*-type 5Q correlators, respectively. Note that they agree with each other within the statistical error. The open symbols refer to the direct lattice QCD data. Since these data behave almost linearly in m_π^2, we adopt the linear chiral extrapolation in m_π^2 to obtain m_{5Q} in the physical quark mass region. Note that the ordinary nonpseudoscalar mesons and baryons show similar linearity in m_π^2 [71]. The closed symbols denote the results of the chiral extrapolation. We see that all the 5Q states appear above the s-wave NK^* and the d-wave NK

TABLE IV. m_{5Q} for each value of κ in the physical unit GeV. The second column labeled by "I.F." indicates the interpolating field used, i.e., (a) the NK^* type, (b) the twisted NK^* type, and (c) the diquark type. $\kappa_{\text{phys.}} \simeq 0.1261$ denotes the value of κ which achieves $m_\pi \simeq 0.14$ GeV. "$\cdots$" indicates that the fitting is not performed due to the large statistical error.

J^P	I.F.	$\kappa = 0.1210$	0.1220	0.1230	0.1240	$\kappa_{\text{phys.}}$
$3/2^-$	(a)	3.08(1)	2.90(2)	2.72(2)	2.54(3)	2.17(4)
$3/2^-$	(b)	3.08(1)	2.89(1)	2.70(2)	2.49(3)	2.11(4)
$3/2^-$	(c)	$\cdots$	$\cdots$	$\cdots$	$\cdots$	$\cdots$
$3/2^+$	(a)	3.52(2)	3.34(3)	3.17(11)	3.00(5)	2.64(7)
$3/2^+$	(b)	3.27(3)	3.11(4)	2.95(5)	2.83(9)	2.48(10)
$3/2^+$	(c)	3.34(2)	3.16(2)	2.98(3)	2.78(5)	2.42(6)

thresholds. As a result of the chiral extrapolation, we obtain only massive 5Q states as $m_{5Q} = 2.17(4)$, 2.11(4) GeV from the NK^*-type and the twisted NK^*-type correlators, respectively, which is too heavy to be identified with the $\Theta^+(1540)$ observed experimentally. Numerical values of m_{5Q} at each hopping parameter together with their chirally extrapolated values are summarized in Table IV. To obtain a low-lying state at $m_{5Q} \simeq 1540$ MeV, a 5Q state should appear below these thresholds at least in the light quark mass region. In this case, a significantly large chiral effect is required. This point may be clarified in the future by an explicit lattice QCD calculation with chiral fermions.

B. $J^P = 3/2^+$ 5Q spectrum with PBC

We consider the spectrum of $J^P = 3/2^+$ pentaquarks. $J^P = 3/2^+$ is an interesting quantum number from the viewpoint of the diquark picture of Jaffe and Wilczek [22]. In this picture, the pair of diquarks has an angular momentum of 1, which is combined with the spin 1/2 of the $\bar{s}$ quark. Hence, there are two possibilities as $J^P = 1/2^+$ and $3/2^+$, i.e., the diquark picture can support the $J^P = 3/2^+$ possibility as well. The mass splitting between the $J^P = 1/2^+$ and $J^P = 3/2^+$ states depends on properties of the LS interaction. If the $J^P = 3/2^+$ state is massive, it is expected to have a large decay width. If it is light enough, its exotic structure may give an explanation to its narrow decay width as for the $J^P = 1/2^+$ case.

In Fig. 3, we show the 5Q effective mass plots with PBC employing three types of interpolating fields, i.e., (a) the NK^* type, (b) the twisted NK^* type, and (c) the diquark type. The dotted lines indicate the s-wave N^*K^*, the p-wave NK^*, and the p-wave NK thresholds in the spatial lattice of size $L \simeq 2.15$ fm, respectively.

Figure 3(a) shows the 5Q effective mass plot employing the NK^*-type interpolating field. In the region, $0 \leq \tau \lesssim 17$, the contaminations of higher spectral contributions are gradually reduced. There is a flat region $18 \lesssim \tau \lesssim 30$, which is still afflicted with slightly large statistical errors. The single-exponential fit in this region gives $m_{5Q} = 3.34(3)$ GeV. Note that this value agrees with the s-wave N^*K^* threshold $E_{th} \simeq 3.27$ GeV (see Table III for m_{N^*}).

Figure 3(b) shows the 5Q effective mass plot corresponding to the twisted NK^*-type interpolating field. We have a rather stable plateau in the interval $21 \leq \tau \leq 27$, where the single-exponential fit is performed. We obtain $m_{5Q} = 3.11(4)$ GeV. The result is denoted by the solid line.

Figure 3(c) shows the 5Q effective mass plot for the diquark-type interpolating field. We find a plateau in the interval $19 \leq \tau \leq 29$. A single-exponential fit gives $m_{5Q} = 3.16(2)$ GeV.

Now, we perform the chiral extrapolation. In Fig. 4, m_{5Q} is plotted against m_π^2. Circles, squares, and triangles denote the data obtained from the NK^*-type, the twisted
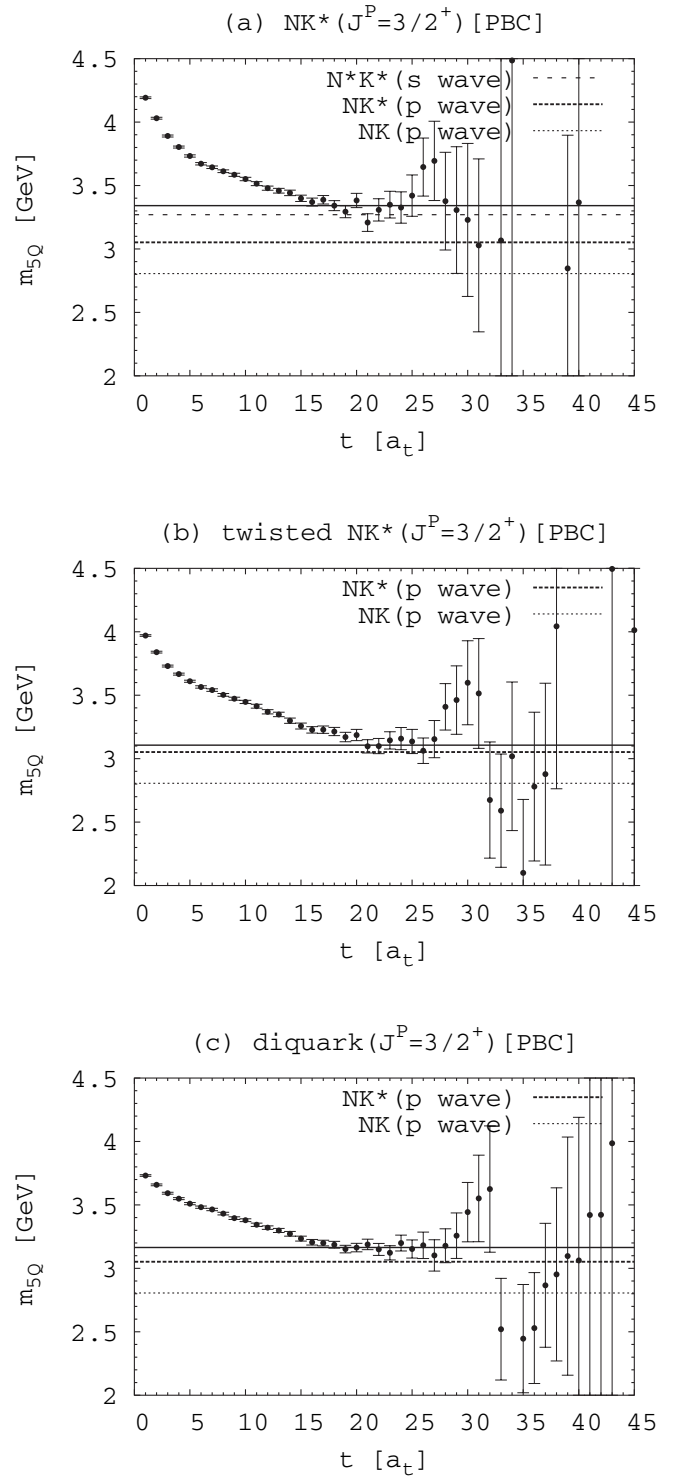

FIG. 3. The 5Q effective mass plots in the $J^P = 3/2^+$ channel with PBC for three types of interpolating fields, i.e., (a) the NK^* type, (b) the twisted NK^* type, and (c) the diquark type. Equation (31) is adopted as a typical set of hopping parameters. The dotted lines indicate the s-wave N^*K^*, the p-wave NK^*, and the p-wave NK thresholds in the spatial lattice size $L \simeq 2.15$ fm. The solid lines denote the results of the single-exponential fit performed in each plateau region.
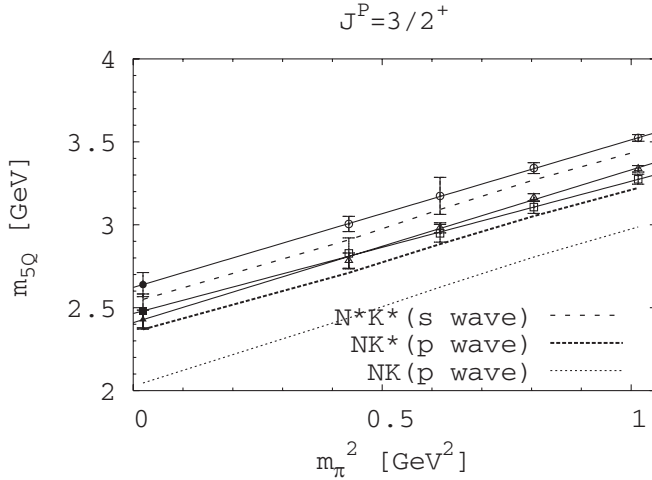
FIG. 4. m_{5Q} in the $J^P = 3/2^+$ channel against m_π^2 for the three interpolating fields, i.e., (circle) the NK^* type, (square) the twisted NK^* type, and (triangle) a diquark type [Eq. (3)]. Open symbols denote the direct lattice QCD data, while the closed symbols and the solid lines represent the results of the chiral extrapolations to the physical quark mass region.

NK^*-type, and the diquark-type 5Q correlators, respectively. Note that the latter two agree with each other within the statistical errors.

As a result of the chiral extrapolation, we obtain $m_{5Q} = 2.64(7)$ GeV from the NK^*-type correlator, $m_{5Q} = 2.48(10)$ GeV from the twisted NK^*-type correlator, and $m_{5Q} = 2.42(6)$ GeV from the diquark-type correlator. Numerical values of m_{5Q} in the $J^P = 3/2^+$ channel at each hopping parameter together with their chirally extrapolated values are also summarized in Table IV. The data from the twisted NK^*-type and the diquark-type correlators are considered to be consistent with the p-wave NK^* threshold, while the data from the NK^*-type correlator seem to correspond to a more massive state, which is likely to be consistent with the N^*K^* (s-wave) threshold. We see again that all of our data of m_{5Q} appear above the NK^* threshold (p wave), which is located above the artificially raised NK threshold (p wave) due to the finiteness of the spatial lattice as $L \simeq 2.15$ fm. As a result, we are left only with massive 5Q states.

Now, several comments are in order. (1) Reference [67] reported the existence of a low-lying 5Q state in the $J^P = 3/2^+$ channel using the NK^*-type interpolating field. However, we have not observed such a low-lying 5Q state in our calculation. There are a number of differences in the lattice QCD setup between the current studies and Ref. [67], such as the gauge and the quark actions, and the implementation of the smeared source. However, we consider that, rather than being a consequence of these differences, the discrepancy mainly comes from the low statistics adopted in Ref. [67]. We emphasize again that spin 3/2 pentaquark correlators are quite noisy, and therefore require better statistics. (2) Recall that, except for a

single calculation [59], lattice QCD calculations indicate that the $J^P = 1/2^+$ state is heavy [57,58,60–66], for instance $m_{5Q} \simeq 2.25$ GeV in Ref. [61]. From the viewpoint of the diquark picture, it could be natural to obtain such massive 5Q states in the $J^P = 3/2^+$ channel. If there were a low-lying 5Q state in the $J^P = 3/2^+$ channel, then the diquark picture could suggest also a low-lying 5Q state in the $J^P = 1/2^+$ channel nearby.

V. ANALYSIS WITH HBC

In the previous section, we have observed only massive 5Q states, which are obtained by using the linear chiral extrapolation in m_π^2. However, the chiral behavior may deviate from a simple linear one in the light quark mass region, which could lead to somewhat less massive states. Considering this, it is worthwhile at this stage to analyze whether our 5Q states are compact 5Q resonances or not. This is done by switching the spatial periodic BC to the hybrid BC introduced in Sec. II.

A. $J^P = 3/2^-$ 5Q spectrum with HBC

Figure 5 shows the 5Q effective mass plots with HBC employing the three types of interpolating fields, i.e., (a) the NK^* type, (b) the twisted NK^* type, and (c) the diquark type. These figures should be compared with their PBC counterparts in Fig. 1. The dotted lines denote the s-wave NK^* and the d-wave NK thresholds. For the typical set of hopping parameters, i.e., Eq. (31), the s-wave NK^* threshold (the thick dotted line) is raised by $\sim$180 MeV, and the d-wave NK threshold (the thin dotted line) is lowered by $\sim$70 MeV due to HBC in the finite spatial extent as $L \simeq 2.15$ fm (see Table I).

Figure 5(a) shows the 5Q effective mass plot for the NK^*-type interpolating field with HBC. We find a plateau in the interval $23 \leq \tau \leq 35$, where the single-exponential fit is performed leading to $m_{5Q} = 2.98(1)$ GeV, which is denoted by the solid line. We see that m_{5Q} is raised by 80 MeV due to HBC. The value of m_{5Q} is consistent with the s-wave NK^* threshold within the statistical error. Therefore, we regard this state as an NK^* scattering state.

Figure 5(b) shows the 5Q effective mass plot for the twisted NK^*-type interpolating field. We find a plateau in the interval $24 \leq \tau \leq 35$, where the single-exponential fit is performed leading to $m_{5Q} = 2.98(1)$ GeV, which is denoted by the solid line. The situation is similar to the NK^*-interpolating field case. We see that m_{5Q} is raised by 90 MeV due to HBC. Since the value is consistent with the s-wave NK^* threshold within the statistical error, we regard it as an NK^* scattering state.

Figure 5(c) shows the 5Q effective mass plot for the diquark-type interpolating field. We see that it is afflicted with a considerable size of statistical errors as before, due to which the best fit is not performed.
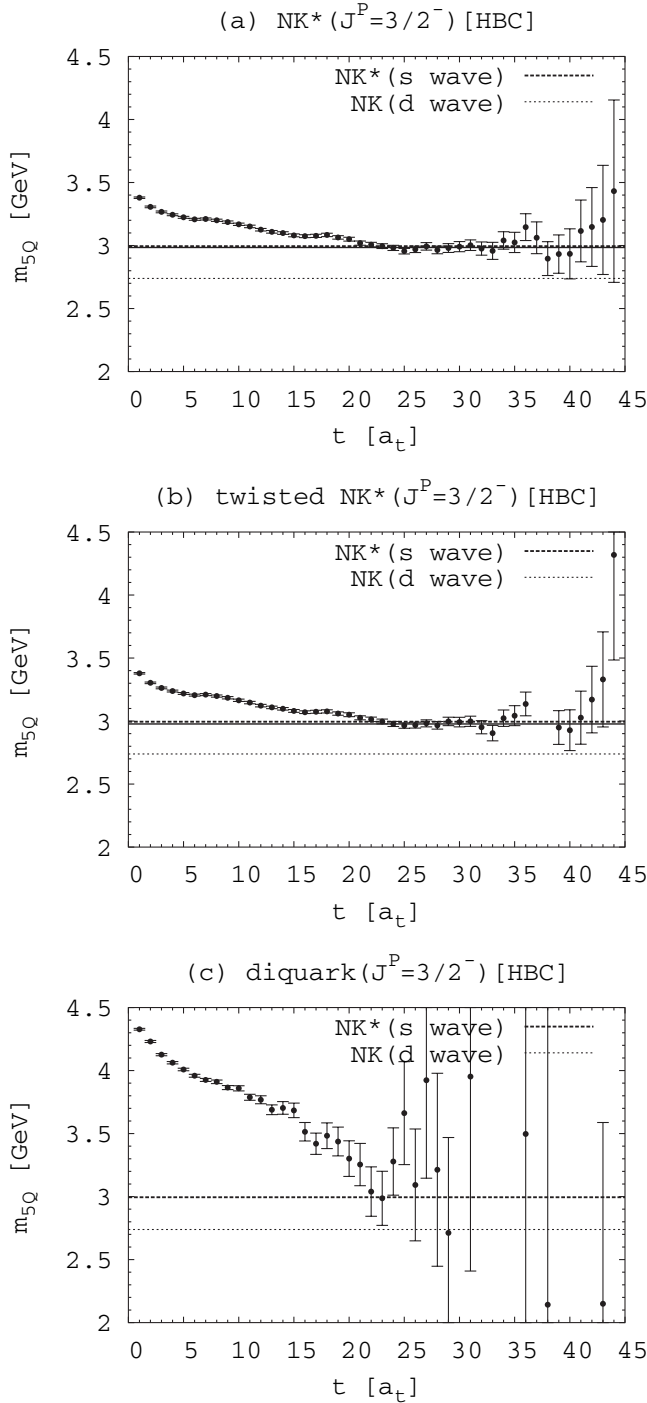
(a) NK⋆(J^P=3/2⁻)[HBC]

(b) twisted NK⋆(J^P=3/2⁻)[HBC]

(c) diquark(J^P=3/2⁻)[HBC]

FIG. 5. The 5Q effective mass plots in the $J^P = 3/2^-$ channel with HBC for three types of interpolating fields, i.e., (a) the NK^* type, (b) the twisted NK^* type, and (c) the diquark type. The meanings of the dotted lines and the solid lines are the same as in Fig. 1.

In this way, all of our 5Q states in the $J^P = 3/2^-$ channel turn out to be NK^* scattering states. More precisely, we do not observe any compact 5Q resonance states in the $J^P = 3/2^-$ channel below the raised s-wave NK^* threshold,

$$E \lesssim \sqrt{m_N^2 + \vec{p}_{\min}^2} + \sqrt{m_{K^*}^2 + \vec{p}_{\min}^2}, \qquad (34)$$

with $|\vec{p}_{\min}| \simeq 499$ MeV.

B. $J^P = 3/2^+$ 5Q spectrum with HBC

Figure 6 shows the 5Q effective mass plots with HBC employing the three types of interpolating fields, i.e., (a) the NK^* type, (b) the twisted NK^* type, and (c) the diquark type. These figures should be compared with their PBC counterparts in Fig. 3. The meaning of the dotted and the solid lines is the same as in Fig. 3.

HBC may not be useful for the $J^P = 3/2^+$ channel, since it induces only minor changes in the two-particle spectra. For the typical set of hopping parameters, i.e., Eq. (31), the p-wave NK^* threshold is lowered only by ~ 60 MeV, and the p-wave NK threshold is lowered only by ~ 70 MeV. We see that these shifts are rather small. This is because they are induced by the changes in the minimum nonvanishing momentum, i.e., $|\vec{p}_{\min}| = 2\pi/L \simeq 576$ MeV to $\sqrt{3}\pi/L \simeq 499$ MeV as mentioned before. In the $J^P = 3/2^+$ channel, N^*K^* (s-wave) threshold shows the most drastic change, i.e., the upper shift by 170 MeV, which however plays a less significant role, since its location is at rather high energy.

Figure 6(a) shows the 5Q effective mass plot employing the NK^*-type interpolating field. There is a flat region $16 \lesssim \tau \lesssim 25$, which is still afflicted with slightly large statistical errors. The single-exponential fit in this region leads to $m_{5Q} = 3.38(2)$ GeV. We see that m_{5Q} is raised by 40 MeV. Although the shift of 40 MeV is rather small, m_{5Q} is again almost consistent with the s-wave N^*K^* threshold. Considering its rather large statistical error, this 5Q state is likely to be an s-wave N^*K^* scattering state. To draw a more solid conclusion on this state, it is necessary to improve the statistics.

Figure 6(b) shows the 5Q effective mass plot employing the twisted NK^*-type interpolating field. There is a plateau in the interval $23 \le \tau \le 31$, where we perform the single-exponential fit. The result $m_{5Q} = 3.02(3)$ GeV is denoted by the solid line. We see that m_{5Q} is lowered by 90 MeV, which is considered to be consistent with the shift of the NK^* (p-wave) threshold. Therefore, this state is likely to be an NK^* (p-wave) scattering state.

Figure 6(c) shows the 5Q effective mass plot employing the diquark-type interpolating field. Although the data are slightly noisy, there is a plateau in the interval $23 \le \tau \le 28$. A single-exponential fit in this plateau region leads to $m_{5Q} = 3.08(4)$ GeV. m_{5Q} is lowered by 80 MeV due to HBC. The situation is similar to Fig. 6(b). This state is likely to be an NK^* (p-wave) scattering state.

In this way, all of our 5Q states are likely to be either N^*K^* (s-wave) or NK^* (p-wave) states rather than compact 5Q resonance states. Of course, because HBC induces only minor changes in the 5Q spectrum in the $J^P = 3/2^+$ channel, and also because 5Q correlators still involve a
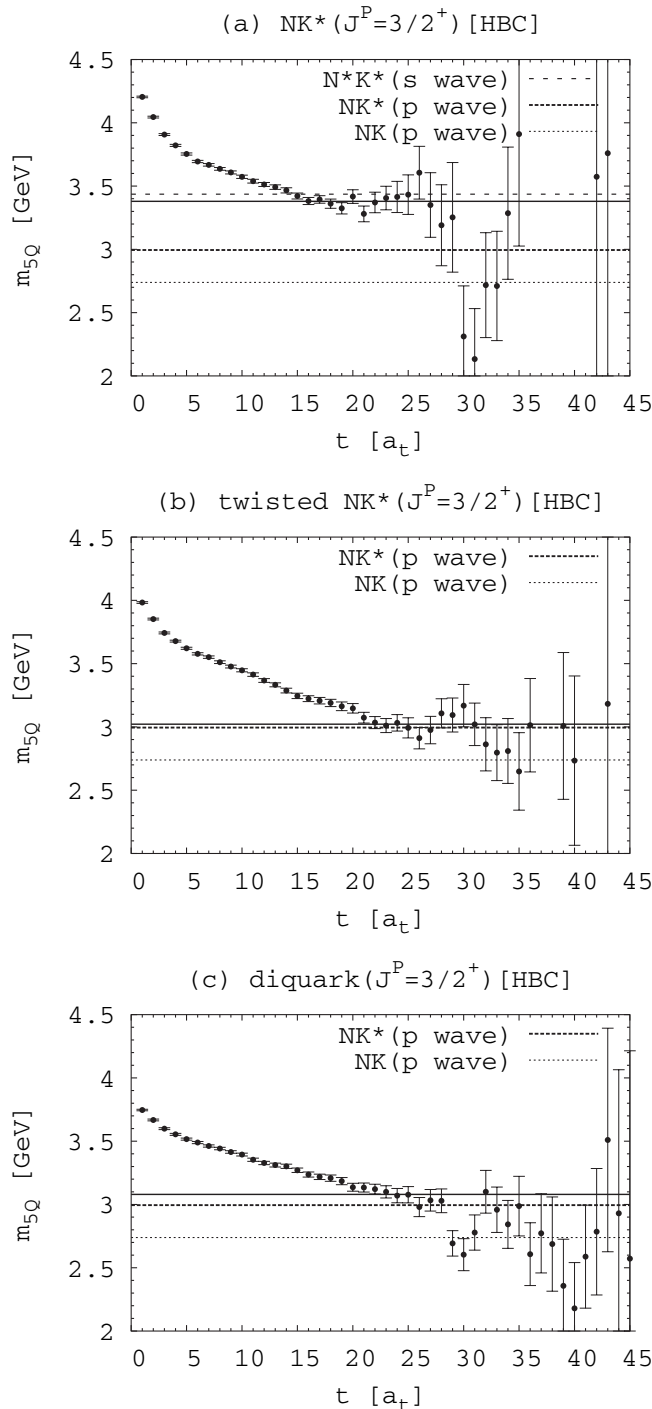
(a) NK*(J^P=3/2^+) [HBC]

(b) twisted NK*(J^P=3/2^+) [HBC]

(c) diquark(J^P=3/2^+) [HBC]

FIG. 6.   5Q effective mass plots in the $J^P = 3/2^+$ channel with HBC for three types of interpolating fields: (a) the NK^* type, (b) the twisted NK^* type, and (c) the diquark type. The meanings of the dotted lines and the solid lines are the same as in Fig. 3.

considerable size of statistical error, more statistics is desirable to draw a solid conclusion on the real nature of these 5Q states. Here, we can at least state that these 5Q states are all massive, which locate above the NK^* (p-wave) threshold.

VI. SUMMARY AND CONCLUSION

High-precision measurements of the masses of the $J^P = 3/2^\pm$ 5Q baryons have been performed in anisotropic lattice QCD at the quenched level with a large number of gauge field configurations as $N_{conf} = 1000$. We emphasize that the spin of $\Theta^+(1540)$ has not yet been determined experimentally, and that the $J^P = 3/2^-$ assignment provides us with one of the possible solutions to the puzzle of the narrow decay width of $\Theta^+(1540)$ [43]. We have employed the standard Wilson gauge action on the anisotropic lattice of the size $12^3 \times 96$ with the renormalized anisotropy $a_s/a_t = 4$ at $\beta = 5.75$, which corresponds to $a_s \simeq 0.18$ fm and $a_t \simeq 0.045$ fm. We have found that correlators of $J^P = 3/2^\pm$ pentaquark baryons are rather noisy. Hence, the large statistics as $N_{conf} = 1000$ has played a key role to get a solid result in our calculation. For the quark part, we have employed $O(a)$-improved Wilson (clover) action with four values of the hopping parameters as $\kappa = 0.1210(0.0010)0.1240$, which roughly cover the region of $m_s \lesssim m \lesssim 2m_s$ for the u-d quark masses. To avoid contaminations of excited states, we have employed the spatially extended smeared source.

We have examined three types of the 5Q interpolating fields: (a) the NK^* type, (b) the (color-)twisted NK^* type, and (c) the diquark type. In the $J^P = 3/2^-$ channel, we have observed plateaus in the effective mass plots for the NK^*-type and the twisted NK^*-type interpolating fields, whereas no plateau has been identified in the ones for the diquark-type interpolating field due to significantly large statistical error. The former two give almost identical results. We have employed the linear chiral extrapolations in m_π^2, which have led to $m_{5Q} \simeq 2.17$ and 2.11 GeV for the NK^*-type and the twisted NK^*-type 5Q correlators, respectively. In the $J^P = 3/2^+$ channel, we have observed plateaus in all three effective mass plots. However, the plateau for the NK^*-type interpolating field is located at a somewhat higher energy than the other two. Chiral extrapolations have led to $m_{5Q} \simeq 2.64$ GeV for the NK^*-type correlator, $m_{5Q} \simeq 2.48$ GeV for the twisted NK^*-type correlator, and $m_{5Q} \simeq 2.42$ GeV for the diquark-type correlator. In this way, our data do not support low-lying 5Q states in both the $J^P = 3/2^\pm$ channels. All the observed 5Q states appear above the d/p-wave NK thresholds, which are higher than the s-wave threshold by a few hundred MeV due to the finiteness of the spatial lattice as $L \simeq 2.15$ fm. Note that a low-lying 5Q state with $J^P = 3/2^\pm$ appears below such NK threshold (p/d wave) at least in the light quark mass region.

In order to clarify whether or not the observed states are compact 5Q resonances, we have performed an analysis using the HBC method, which was recently proposed by Ref. [61]. In the $J^P = 3/2^-$ channel, the observed 5Q states in the NK^*-type and the twisted NK^*-type correlators have turned out to be s-wave NK^* scattering states. In the $J^P = 3/2^+$ channel, for the twisted NK^*-type and the

diquark-type correlators, the observed 5Q states are most likely to be NK^* (*p*-wave) scattering states. For the other one, i.e., the NK^*-type interpolating field, although more statistics is needed to draw a definite conclusion, it is most likely to be an *s*-wave N^*K^* scattering state. Note that, since HBC does not affect the two-particle spectra so much in the $J^P = 3/2^+$ channel, it is not easy to elucidate the nature of the 5Q states only with HBC. At any rate, whatever the real nature of these 5Q states may be, they result in considerably massive states at the physical quark mass, and therefore cannot be identified as $\Theta^+(1540)$ without involving a significantly large chiral contribution.

In conclusion, we have not obtained any relevant signals for low-lying compact 5Q resonance states in the $J^P = 3/2^\pm$ channels below 2.1 GeV in the present study. In order to make this conclusion established, further systematic studies with various quantum numbers in lattice QCD will be helpful. For instance, it is desirable to use (1) unquenched full lattice QCD, (2) finer and larger volume lattice, (3) chiral fermion with small mass, (4) more sophisticated interpolating field corresponding to the diquark picture, and so on. In any case, the mysterious exotic pentaquark is to be clarified in future studies of lattice QCD as well as in future experiments.

ACKNOWLEDGMENTS

APPENDIX: SPECTRAL REPRESENTATION

Considering the importance of the parity determination of Θ^+, we present a brief derivation of the spectral representation of Rarita-Schwinger correlators, i.e., Eq. (8), with Eq. (11). In this section, the gamma matrices are represented in the Minkowskian form (see Ref. [82]). To avoid unnecessary complexities, we derive formulas only for $J^P = 3/2^\pm$. The $J^P = 1/2^\pm$ counterparts can be obtained by a slight modification.

We first consider the coupling of our interpolating fields ψ_μ to a $J^P = 3/2^\pm$ (anti-)baryon state. Because of Eq. (6), our interpolating fields, i.e., Eqs. (1)–(3) have a negative intrinsic parity. Hence, their couplings to $J^P = 3/2^-$ (anti-)baryons are parametrized in the following way:

$$\langle 0|\psi_\mu(0)|B_{3/2^-}(k, \alpha)\rangle = \lambda_{3/2^-} u_\mu(m_{3/2^-}; k, \alpha),$$
$$\langle 0|\bar{\psi}_\mu(0)|\bar{B}_{3/2^-}(k, \alpha)\rangle = \lambda_{3/2^-}^* \bar{v}_\mu(m_{3/2^-}; k, \alpha), \tag{A1}$$

where $|B_{3/2^-}(k, \alpha)\rangle$ [$|\bar{B}_{3/2^-}(k, \alpha)\rangle$] denotes a $J^P = 3/2^-$ (anti-)baryon state with momentum k, helicity α, and mass $m_{3/2^+}$ $(m_{3/2^-})$. $u_\mu(m; k, \alpha)$ and $v_\mu(m; k, \alpha)$ denote the Rarita-Schwinger spinors for $J = 3/2$ particles [73–75]. Equations (1)–(3) couple to $J^P = 3/2^+$ states as well. In that case, their couplings involve γ_5 in the following way:

$$\langle 0|\psi_\mu(0)|B_{3/2^+}(k, \alpha)\rangle = \lambda_{3/2^+} \gamma_5 u_\mu(m_{3/2^+}; k, \alpha),$$
$$\langle 0|\bar{\psi}_\mu(0)|\bar{B}_{3/2^+}(k, \alpha)\rangle = -\lambda_{3/2^+}^* \bar{v}_\mu(m_{3/2^+}; k, \alpha)\gamma_5. \tag{A2}$$

The negative sign for the antibaryon originates from the anticommutativity of γ_0 and γ_5.

To derive the spectral representation, the best way would be to express it in the operator representation in the following way:

$$G_{\mu\nu}(\tau, \vec{x}) = Z^{-1} \text{Tr}(e^{-\beta H} T_\tau[\psi_\mu(\tau, \vec{x})\bar{\psi}_\nu(0)]), \tag{A3}$$

where β denotes the temporal extent of the lattice, $H \equiv H_{\text{QCD}}$ denotes the QCD Hamiltonian, $Z \equiv \text{Tr}(e^{-\beta H})$ denotes the partition function, and $T_\tau[*]$ represents the time-ordered product along the imaginary time direction. The interpolating fields are represented in the Heisenberg picture in imaginary time, i.e., $\psi_\mu(\tau, \vec{x}) = e^{\tau H}\psi_\mu(0, \vec{x})e^{-\tau H}$ and $\bar{\psi}_\mu(\tau, \vec{x}) = e^{\tau H}\bar{\psi}_\mu(0, \vec{x})e^{-\tau H}$. By restricting ourselves to the interval $0 \leq \tau < \beta$, Eq. (A3) reduces to

$$G_{\mu\nu}(\tau, \vec{x}) = \text{Tr}\left(\frac{e^{-\beta H}}{Z} \psi_\mu(\tau, \vec{x})\bar{\psi}_\nu(0)\right). \tag{A4}$$

Note that it can be equivalently expressed as

$$G_{\mu\nu}(\tau, \vec{x}) = \text{Tr}\left(\psi_\mu(\tau - \beta, \vec{x})\frac{e^{-\beta H}}{Z} \bar{\psi}_\nu(0)\right). \tag{A5}$$

In the large β limit, we have $e^{-\beta H}/Z \simeq |0\rangle\langle 0|$, which is inserted into Eqs. (A4) and (A5). Note that the resulting two expressions serve as independent contributions to the original "Tr," i.e., Eq. (A4) [or Eq. (A5)]. Hence, we keep these two contributions to obtain

$$G_{\mu\nu}(\tau, \vec{x}) \simeq \langle 0|\psi_\mu(\tau, \vec{x})\bar{\psi}_\nu(0)|0\rangle$$
$$+ \langle 0|\bar{\psi}_\nu(0)\psi_\mu(\tau - \beta, \vec{x})|0\rangle. \tag{A6}$$

Note that the 1st term corresponds to the forward propagation, whereas the 2nd term to the backward propagation. By inserting single-(anti-)baryon intermediate states, and by using Eqs. (A1) and (A2), we are left with

$$G_{\mu\nu}(\tau,\vec{x}) = \sum_{\alpha=1}^{4} \int \frac{d^3k}{(2\pi)^3} \frac{m_{3/2^+}}{k_0} e^{-\tau k_0} \langle 0|\psi_\mu(\vec{x})|B_{3/2^+}(k,\alpha)\rangle \langle B_{3/2^+}(k,\alpha)|\bar{\psi}_\nu(0)|0\rangle + \cdots$$

$$= |\lambda_{3/2^-}|^2 \int \frac{d^3k}{(2\pi)^3} \frac{m_{3/2^-}}{k_0} (-1) P_{\mu\nu}^{(3/2)}(k) \left[e^{-\tau k_0} e^{i\vec{k}\cdot\vec{x}} \left(\frac{m_{3/2^-} + \not{k}}{2m_{3/2^-}} \right) + e^{-(\beta-\tau)k_0} e^{-i\vec{k}\cdot\vec{x}} \left(\frac{m_{3/2^-} - \not{k}}{2m_{3/2^-}} \right) \right]$$

$$- |\lambda_{3/2^+}|^2 \int \frac{d^3k}{(2\pi)^3} \frac{m_{3/2^+}}{k_0} (-1) P_{\mu\nu}^{(3/2)}(k) \left[e^{-\tau k_0} e^{i\vec{k}\cdot\vec{x}} \left(\frac{m_{3/2^+} - \not{k}}{2m_{3/2^+}} \right) + e^{-(\beta-\tau)k_0} e^{-i\vec{k}\cdot\vec{x}} \left(\frac{m_{3/2^+} + \not{k}}{2m_{3/2^+}} \right) \right], \quad (A7)$$

where $k_0 \equiv \sqrt{m_{3/2^-}^2 + \vec{k}^2}$ for $J^P = 3/2^-$, $k_0 \equiv \sqrt{m_{3/2^+}^2 + \vec{k}^2}$ for $J^P = 3/2^+$, and the following identities are used:

$$\sum_{\alpha=1}^{4} u_\mu(m;k,\alpha)\bar{u}_\nu(m;k,\alpha) = -\frac{m + \not{k}}{2m} P_{\mu\nu}^{(3/2)}(k),$$

$$\sum_{\alpha=1}^{4} v_\mu(m;k,\alpha)\bar{v}_\nu(m;k,\alpha) = \frac{m - \not{k}}{2m} P_{\mu\nu}^{(3/2)}(k), \quad (A8)$$

where $P_{\mu\nu}^{(3/2)}(k)$ is the spin 3/2 projection operator defined as

$$P_{\mu\nu}^{(3/2)}(k) \equiv g_{\mu\nu} - \frac{1}{3}\gamma_\mu\gamma_\nu - \frac{1}{3k^2}(\not{k}\gamma_\mu k_\nu + k_\mu \gamma_\nu \not{k}). \quad (A9)$$

By performing the integration over $\vec{x}$ in order to make zero-momentum projection, and by replacing the Minkowskian gamma matrices by their Euclidean counterparts, we finally arrive at the spectral representation Eq. (8) with Eq. (11).

Derivation of the spin 1/2 parts is similarly done by using the following parametrizations instead of Eqs. (A1)

and (A2),

$$\langle 0|\psi_\mu(0)|B_{1/2^-}(k,\alpha)\rangle = (\lambda_{1/2^-}\gamma_\mu + \lambda'_{1/2^-}k_\mu) \\ \times u(m_{1/2^-};k,\alpha),$$

$$\langle 0|\bar{\psi}_\mu(0)|\bar{B}_{1/2^-}(k,\alpha)\rangle = \bar{v}(m_{1/2^-};k,\alpha) \\ \times (\lambda^*_{1/2^-}\gamma_\mu - \lambda'^*_{1/2^-}k_\mu),$$

$$\langle 0|\psi_\mu(0)|B_{1/2^+}(k,\alpha)\rangle = (\lambda_{1/2^+}\gamma_\mu + \lambda'_{1/2^+}k_\mu) \\ \times \gamma_5 u(m_{1/2^+};k,\alpha),$$

$$\langle 0|\bar{\psi}_\mu(0)|\bar{B}_{1/2^-}(k,\alpha)\rangle = -\bar{v}(m_{1/2^-};k,\alpha) \\ \times \gamma_5(\lambda^*_{1/2^-}\gamma_\mu - \lambda'^*_{1/2^-}k_\mu), \quad (A10)$$

where $|B_{1/2^\pm}(k,\alpha)\rangle$ and $|\bar{B}_{1/2^\pm}(k,\alpha)\rangle$ denote the $J^P = 1/2^\pm$ (anti-)baryon states with momentum k, helicity α, and mass $m_{1/2^\pm}$. $u(m;k,\alpha)$ and $v(m;k,\alpha)$ denote the Dirac bispinors for spin 1/2 particles with mass m, momentum k, and helicity α. $\lambda_{1/2^\pm}$ and $\lambda'_{1/2^\pm}$ represent the couplings to $J^P = 1/2^\pm$ (anti-)baryons.

[1] T. Nakano *et al.* (LEPS Collaboration), Phys. Rev. Lett. **91**, 012002 (2003).

[2] C. Alt *et al.* (NA49 Collaboration), Phys. Rev. Lett. **92**, 042003 (2004).

[3] A. Aktas *et al.* (H1 Collaboration), Phys. Lett. B **588**, 17 (2004).

[4] S. K. Choi *et al.* (Belle Collaboration), Phys. Rev. Lett. **91**, 262001 (2003); D. Acosta *et al.* (CDF II Collaboration), Phys. Rev. Lett. **93**, 072001 (2004); P. Pakhlov (for the Belle Collaboration), hep-ex/0412041; S.-K. Choi *et al.* (Belle Collaboration), Phys. Rev. Lett. **94**, 182002 (2005); T. Suzuki *et al.*, Phys. Lett. B **597**, 263 (2004); B. Aubert *et al.* (*BABAR* Collaboration), Phys. Rev. Lett. **90**, 242001 (2003); S.-K. Choi *et al.* (BELLE Collaboration), Phys. Rev. Lett. **91**, 262002 (2003); D. Besson *et al.* (CLEO Collaboration), Phys. Rev. D **68**, 032002 (2003).

[5] D. Diakonov, V. Petrov, and M. V. Polyakov, Z. Phys. A **359**, 305 (1997).

[6] R. L. Jaffe, SLAC Report No. SLAC-PUB-1774, 1976.

[7] D. Strottman, Phys. Rev. D **20**, 748 (1979).

[8] H. Weigel, Eur. Phys. J. A **2**, 391 (1998).

[9] M. Praszalowicz, Phys. Lett. B **575**, 234 (2003); in *Proceedings of the Workshop on Skyrmions and Anomalies, Mogilany, Poland, 1987*, edited by M. Jezabek and M. Praszalowicz (World Scientific, Singapore, 1987), p. 112.

[10] V. V. Barmin *et al.* (DIANA Collaboration), Phys. At. Nucl. **66**, 1715 (2003).

[11] S. Stepanyan *et al.* (CLAS Collaboration), Phys. Rev. Lett. **91**, 252001 (2003).

[12] J. Barth *et al.* (SAPHIR Collaboration), Phys. Lett. B **572**, 127 (2003).

[13] A. E. Asratyan, A. G. Dolgolenko, and M. A. Kubantsev, Phys. At. Nucl. **67**, 682 (2004); V. Kubarovsky *et al.* (CLAS Collaboration), Phys. Rev. Lett. **92**, 032001 (2004); A. Airapetian *et al.* (HERMES Collaboration), Phys. Lett. B **585**, 213 (2004); A. Aleev *et al.* (SVD Collaboration), hep-ex/0401024; M. Abdel-Bary *et al.*

(COSY-TOF Collaboration), Phys. Lett. B **595**, 127 (2004); S. Chekanov *et al.* (ZEUS Collaboration), Phys. Lett. B **591**, 7 (2004).

[14] J. Z. Bai *et al.* (BES Collaboration), Phys. Rev. D **70**, 012004 (2004); K. T. Knoepfle *et al.* (HERA-B Collaboration), J. Phys. G **30**, S1363 (2004); C. Pinkenburg *et al.* (PHENIX Collaboration), J. Phys. G **30**, S1201 (2004); I. Abt *et al.* (HERA-B Collaboration), Phys. Rev. Lett. **93**, 212003 (2004); Yu. M. Antipov *et al.* (SPHINX Collaboration), Eur. Phys. J. A **21**, 455 (2004); I. V. Gorelov *et al.* (CDF Collaboration), hep-ex/0408025; M. J. Longo *et al.* (HyperCP Collaboration), Phys. Rev. D **70**, 111101 (2004); B. Aubert *et al.* (*BABAR* Collaboration), hep-ex/0408064; S. R. Armstrong, Nucl. Phys. B, Proc. Suppl. **142**, 364 (2005); K. Abe *et al.* (BELLE Collaboration), hep-ex/0409010; S. Schael *et al.* (ALEPH Collaboration), Phys. Lett. B **599**, 1 (2004); D. O. Litvintsev *et al.* (CDF Collaboration), Nucl. Phys. B, Proc. Suppl. **142**, 374 (2005); K. Stenson *et al.* (FOCUS Collaboration), Int. J. Mod. Phys. A **20**, 3745 (2005); R. Mizuk *et al.* (BELLE Collaboration), hep-ex/0411005.

[15] For a recent review of the experimental status, K. H. Hicks, Prog. Part. Nucl. Phys. **55**, 647 (2005), and references therein.

[16] M. Oka, Prog. Theor. Phys. **112**, 1 (2004), and references therein.

[17] S. L. Zhu, Int. J. Mod. Phys. A **19**, 3439 (2004), and references therein.

[18] T. D. Cohen, Phys. Lett. B **581**, 175 (2004).

[19] N. Itzhaki, I. R. Klebanov, P. Ouyang, and L. Rastelli, Nucl. Phys. **B684**, 264 (2004).

[20] H.-Ch. Kim, Phys. Lett. B **585**, 99 (2004).

[21] A. Hosaka, Phys. Lett. B **571**, 55 (2003).

[22] R. L. Jaffe and F. Wilczek, Phys. Rev. Lett. **91**, 232003 (2003).

[23] M. Karliner and H. J. Lipkin, Phys. Lett. B **575**, 249 (2003).

[24] C. E. Carlson, C. D. Carone, H. J. Kwee, and V. Nazaryan, Phys. Lett. B **579**, 52 (2004).

[25] Fl. Stancu and D. O. Riska, Phys. Lett. B **575**, 242 (2003).

[26] B. K. Jennings and K. Maltman, Phys. Rev. D **69**, 094020 (2004).

[27] L. Y. Glozman, Phys. Lett. B **575**, 18 (2003).

[28] Y. Kanada-Enyo, O. Morimatsu, and T. Nishikawa, Phys. Rev. C **71**, 045202 (2005).

[29] P. Bicudo and G. M. Marques, Phys. Rev. D **69**, 011503 (2004).

[30] F. J. Llanes-Estrada, E. Oset, and V. Mateu, Phys. Rev. C **69**, 055203 (2004).

[31] C. E. Carlson, C. D. Carone, H. J. Kwee, and V. Nazaryan, Phys. Lett. B **573**, 101 (2003).

[32] F. Huang, Z. Y. Zhang, Y. W. Yu, and B. S. Zou, Phys. Lett. B **586**, 69 (2004).

[33] T. Shinozaki, M. Oka, and S. Takeuchi, Phys. Rev. D **71**, 074025 (2005).

[34] S.-L. Zhu, Phys. Rev. Lett. **91**, 232002 (2003).

[35] R. D. Matheus, F. S. Navarra, M. Nielsen, R. Rodrigues da Silva, and S. H. Lee, Phys. Lett. B **578**, 323 (2004).

[36] J. Sugiyama, T. Doi, and M. Oka, Phys. Lett. B **581**, 167

[37] Y. Oh, H. Kim, and S. H. Lee, Phys. Rev. D **69**, 094009 (2004).

[38] Y. Maezawa, T. Maruyama, N. Itagaki, and T. Hatsuda, Acta Phys. Hung. A **22**, 61 (2005).

[39] I. M. Narodetskii, Yu. A. Simonov, M. A. Trusov, and A. I. Veselov, Phys. Lett. B **578**, 318 (2004).

[40] M. Bando, T. Kugo, A. Sugamoto, and S. Terunuma, Prog. Theor. Phys. **112**, 325 (2004).

[41] H. Suganuma, H. Ichie, F. Okiharu, and T. T. Takahashi, in *Proceedings of the International Workshop "PENTAQUARK04"* (World Scientific, Singapore, 2005), p. 414.

[42] F. Okiharu, H. Suganuma, and T. T. Takahashi, Phys. Rev. Lett. **94**, 192001 (2005); Phys. Rev. D **72**, 014505 (2005); H. Suganuma, T. T. Takahashi, F. Okiharu, and H. Ichie, in *Proceedings of the QCD Down Under, Adelaide, 2004* [Nucl. Phys. B, Proc. Suppl. **141**, 92 (2005)].

[43] A. Hosaka, M. Oka, and T. Shinozaki, Phys. Rev. D **71**, 074021 (2005).

[44] T. Nishikawa, Y. Kanada-En'yo, and O. Morimatsu, Phys. Rev. D **71**, 076004 (2005).

[45] S. Takeuchi and K. Shimizu, Phys. Rev. C **71**, 062202 (2005).

[46] J. Sugiyama, T. Doi, and M. Oka (private communication).

[47] W. Wei, P.-Z. Huang, H.-X. Chen, and S.-L. Zhu, J. High Energy Phys. 07 (2005) 015.

[48] T. Inoue, V. E. Lyubovitskij, Th. Gutsche, and A. Faessler, hep-ph/0407305.

[49] R. Jaffe and F. Wilczek, Phys. Rev. D **69**, 114017 (2004).

[50] F. Huang, Z. Y. Zhang, and Y. W. Yu, hep-ph/0411222.

[51] S. Capstick, P. R. Page, and W. Roberts, Phys. Lett. B **570**, 185 (2003).

[52] J. J. Dudek and F. E. Close, Phys. Lett. B **583**, 278 (2004).

[53] T. Hyodo and A. Hosaka, Phys. Rev. D **71**, 054017 (2005).

[54] S. I. Nam, A. Hosaka, and H.-C. Kim, hep-ph/0505134.

[55] S. Eidelman *et al.* (Particle Data Group), Phys. Lett. B **592**, 1 (2004).

[56] T. Kishimoto and T. Sato, hep-ex/0312003.

[57] F. Csikor, Z. Fodor, S. D. Katz, and T. G. Kovacs, J. High Energy Phys. 11 (2003) 070.

[58] S. Sasaki, Phys. Rev. Lett. **93**, 152001 (2004).

[59] T. W. Chiu and T. H. Hsieh, Phys. Rev. D **72**, 034505 (2005).

[60] N. Mathur, F. X. Lee, A. Alexandru, C. Bennhold, Y. Chen, S. J. Dong, T. Draper, I. Horváth, K. F. Liu, S. Tamhankar, and J. B. Zang, Phys. Rev. D **70**, 074508 (2004).

[61] N. Ishii, T. Doi, H. Iida, M. Oka, F. Okiharu, and H. Suganuma, Phys. Rev. D **71**, 034001 (2005).

[62] T. T. Takahashi, T. Umeda, T. Onogi, and T. Kunihiro, Phys. Rev. D **71**, 114509 (2005).

[63] B. G. Lasscock, J. Hedditch, D. B. Leinweber, W. Melnitchouk, A. W. Thomas, A. G. Willams, R. D. Young, and J. M. Zanotti, Phys. Rev. D **72**, 014502 (2005).

[64] C. Alexandrou and A. Tsapalis, hep-lat/0503013.

[65] F. Csikor, Z. Fodor, S. D. Katz, T. G. Kovács, and B. C. Tóth, hep-lat/0503012.

[66] K. Holland and K. J. Juge, hep-lat/0504007.
[67] B. G. Lasscock, D. B. Leinweber, W. Melnitchouk, A. W. Thomas, A. G. Williams, R. D. Young, and J. M. Zanotti, hep-lat/0504015.
[68] G. T. Fleming, J. Phys. Conf. Ser. **9**, 226 (2005).
[69] T. R. Klassen, Nucl. Phys. **B533**, 557 (1998).
[70] H. Matsufuru, T. Onogi, and T. Umeda, Phys. Rev. D **64**, 114503 (2001).
[71] Y. Nemoto, N. Nakajima, H. Matsufuru, and H. Suganuma, Phys. Rev. D **68**, 094505 (2003).
[72] N. Ishii, H. Suganuma, and H. Matsufuru, Phys. Rev. D **66**, 094506 (2002); **66**, 014507 (2002).
[73] B. L. Ioffe, Nucl. Phys. **B188**, 317 (1981).
[74] M. Benmerrouche, R. M. Davidson, and N. C. Mukhopadhyay, Phys. Rev. C **39**, 2339 (1989).

[75] T. R. Hemmert, B. R. Holstein, and J. Kambor, J. Phys. G **24**, 1831 (1998).
[76] I. Montvay and G. Münster, *Quantum Fields on a Lattice* (Cambridge University Press, Cambridge, UK, 1994), p. 1.
[77] R. L. Jaffe, Nucl. Phys. B, Proc. Suppl. **142**, 343 (2005).
[78] N. Ishii, T. Doi, H. Iida, Y. Nemoto, M. Oka, F. Okiharu, and H. Suganuma, ''Penta Quark in Anisotropic Lattice QCD'' (unpublished).
[79] S. Hashimoto, Phys. Rev. D **50**, 4639 (1994).
[80] S. Aoki *et al.* (CP-PACS Collaboration), Phys. Rev. Lett. **84**, 238 (2000).
[81] A. A. Khan *et al.* (CP-PACS Collaboration), Phys. Rev. D **65**, 054505 (2002).
[82] C. Itzykson and J.-B. Zuber, *Quantum Field Theory* (McGraw-Hill, Singapore, 1985), p. 45.